Fraunhofer Diffraction by Ice Crystals Suspended in the Atmosphere

By Yoshihide Takano

Upper Atmosphere Research Laboratory, Tohoku University, Sendai 980, Japan

and

Shoji Asano

Meteorological Research Institute, Tsukuba, Ibaraki 305, Japan

(Manuscript received 18 October 1982, in revised form 8 February 1983)

Abstract

Fraunhofer diffraction has been explicitly formulated for a finite hexagonal cylinder and a spheroid in any arbitrary orientation. The diffracted intensity was computed for hexagonal cylinders and spheroids oriented randomly in a three dimensional space and in a horizontal plane. The diffraction by hexagonal cylinders in 3D random orientation can be well approximated by that of spheroids of the same aspect ratio. For horizontal orientation, the diffracted intensity is a function not only of the scattering angle but also of the azimuth angle, and the diffraction patterns for hexagonal cylinders and spheroids are quite different from each other. The diffraction patterns of hexagonal cylinders in horizontal orientation strongly depend on the source elevation, showing patterns highly anisotropic with respect to the azimuth angle at low source elevations. Applications to optical phenomena due to ice crystals in the atmosphere are also discussed.

1. Introduction

An exact treatment of the light scattering by ice crystals in the atmosphere seems to be impracticable, if not impossible. However, since sizes of ice crystals are much larger than the wavelength of light, the scattering can be described by the geometrical optics approximation. In addition, predominant shape of ice crystals can be well modelled by hexagonal plates and hexagonal columns: hereafter we shall refer to both as hexagonal cylinders. Recent years, several attempts have been made to investigate the light scattering by hexagonal cylinders by means of the geometrical optics approximation (Jacobowitz, 1971; Wendling *et al.*, 1979; Coleman and Liou, 1981; Cai and Liou, 1982).

In geometrical optics approximation, the scattered light is decomposed into light rays diffracted, externally (Fresnel) reflected, and refracted after some internal reflections. The diffraction of the sun or moon light by ice crystals can be described by the Fraunhofer diffraction theory since the light source and the observer are both very far from the targets. In earlier studies, the Fraunhofer diffraction by hexagonal cylinders was approximated by that for rectangular or circular apertures (Jacobowitz, 1971; Wendling *et al.*, 1979). More recently, Coleman and Liou (1981), and Cai and Liou (1982) have treated more exactly the diffraction by finite hexagonal cylinders; unfortunately their formulations contain some minor oversights, and hence differ from our formulation presented in this work.

In the present study, we shall concentrate ourselves on the diffraction by hexagonal cylinders and spheroids. First, the Fraunhofer diffraction by these particles in an arbitrary orientation is explicitly formulated. Then the diffracted intensity is computed for those particles oriented randomly in a 3D space as well as in a horizontal plane. The small roughness and the skeleton structure of ice crystals will not appreciably affect the diffracted intensity distribution, so that we can treat only convex ice crystal particles without losing generality.

Ice crystals in the atmosphere present various optical phenomena such as the 22° halo, parhelia, light pillar, and so on. Quite frequently anisotropic light scattering patterns like an asteroid or a cross are observed in the vicinity of the light source. We shall discuss some relations

between the diffraction patterns of hexagonal cylinders and the optical phenomena due to ice crystals in horizontal orientation.

2. Theory

In order to study the diffraction by a particle, we apply Babinet's principle (van de Hulst, 1957; Born and Wolf, 1975), which states that the distribution of light intensity diffracted by a particle is identical with that by an aperture of the shape and size identical to the geometric shadow of the particle. In the limit of Fraunhofer diffraction at the far field, the disturbance amplitude of diffraction by an aperture S at an arbitrary point $P(\theta, \phi)$ is given, ignoring a constant factor, by (Born and Wolf, 1975)

$$A=k^2\iint_S \exp[-i(Xx'+Yy')]dx'dy', \quad (1)$$

where

$$X=k\sin\theta\cos\phi,$$
$$Y=k\sin\theta\sin\phi. \quad (2)$$

Here k is the wave number of the incident plane wave, $i=\sqrt{-1}$, θ is the scattering angle, and ϕ is the azimuth angle. The diffracted intensity I is given by the square of the absolute value of the amplitude of disturbance, viz., $I=|A|^2$.

A. Diffraction by a hexagonal cylinder

Let a plane wave be incident on a hexagonal cylinder from a direction with zenith angle $(\pi/2-\alpha)$ and azimuth angle β measured with respect to the coordinate system fixed to the cylinder, where the x- and z-axes are directed, respectively, along the a- and c-axes of the hexagonal cylinder. The origin O of the coordinate system is taken at the center of the cylinder. The geometric shadow of the hexagonal cylinder projected onto a plane normal to the incident direction is expressed in terms of the (x', y') coordinates of its marginal vertexes in a new coordinate system, whose z' axis is taken along the incident direction (see Fig. 1). The transformation of the body-framed coordinate system $X(x, y, z)$ into the new coordinate system $X'(x', y', z')$ can be written in the form:

$$X'=BCDX, \quad (3)$$

where the transformation matrixes are given by

$$B=\begin{pmatrix}\cos\phi & \sin\phi & 0\\ -\sin\phi & \cos\phi & 0\\ 0 & 0 & 1\end{pmatrix}, \quad (4)$$

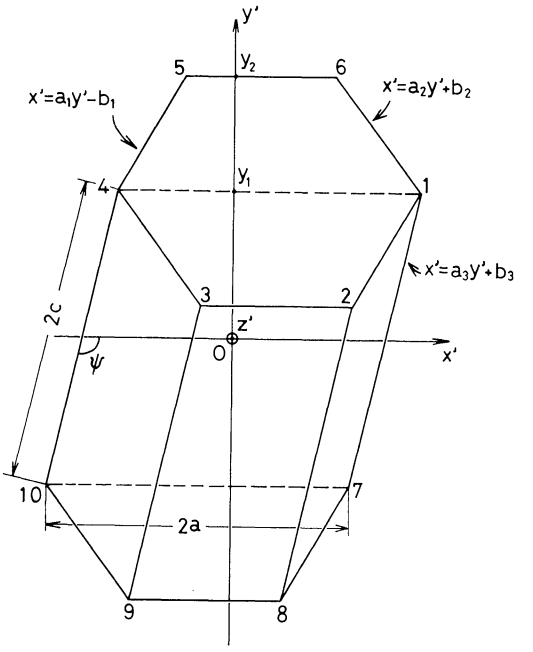

Fig. 1 Geometric shadow of a hexagonal cylinder projected onto a plane normal to the incident direction.

$$C=\begin{pmatrix}\sin\alpha & 0 & -\cos\alpha\\ 0 & 1 & 0\\ \cos\alpha & 0 & \sin\alpha\end{pmatrix}, \quad (5)$$

$$D=\begin{pmatrix}\cos\beta & \sin\beta & 0\\ -\sin\beta & \cos\beta & 0\\ 0 & 0 & 1\end{pmatrix}, \quad (6)$$

with

$$\tan\phi=-\tan(\beta+\pi/3)/\sin\alpha,$$
$$(0\leqq\phi\leqq\pi). \quad (7)$$

Therefore, if the size and shape of the hexagonal cylinder as well as the propagation direction (α, β) of the incident wave are known, the coefficients a_1, a_2, a_3, b_1, b_2, b_3, y_1 and y_2 in Fig. 1 are easily determined by Eq. (3). Here we specify the size and shape of the cylinder by, respectively, ka and the length to radius ratio c/a; a and c are the half-lengths of the a- and c-axes of the hexagonal cylinder, respectively.

The integration of Eq. (1) over the geometric shadow area bounded by (1-6-5-4-10-9-8-7-1) in Fig. 1 can be easily performed by dividing the whole integration domain into three subdomains: two trapezoids (1-6-5-4-1) and (7-10-9-8-7), and one parallelogram (1-4-10-7-1). The operation of the matrix B in Eq. (3) is done to make the bases

of the trapezoids parallel to the x' axis, so that we can apply the integration method by Smith and Marsh (1974). Finally we have the diffraction amplitude A_H of a hexagonal cylinder in the orientation (α, β) at a point $P(\theta, \phi)$ in the form:

$$\begin{aligned} &A_H(\theta, \phi; \alpha, \beta; ka, c/a) \\ &= \frac{4k^2}{X(a_1X+Y)} \sin\left[\frac{1}{2}(y_2-y_1)(a_1X+Y)\right] \\ &\times \sin\left\{\frac{1}{2}[-a_1(y_1+y_2)+2b_1]X \right. \\ &\left. -\frac{1}{2}(y_1+y_2)Y\right\} + \frac{4k^2}{X(a_2X+Y)} \\ &\times \sin\left[\frac{1}{2}(y_2-y_1)(a_2X+Y)\right] \\ &\times \sin\left\{\frac{1}{2}[a_2(y_1+y_2)+2b_2]X+\frac{1}{2}(y_1+y_2)Y\right\} \\ &+ \frac{4k^2}{X(a_3X+Y)} \sin[y_1(a_3X+Y)]\sin(b_3X)\,. \end{aligned} \tag{8}$$

B. Diffraction by a spheroidal particle

The geometric shadow of a spheroid projected onto a plane perpendicular to the incident direction is, in general, an ellipse. We specify an orientation of a spheroid by an angle ζ between the incident direction and the rotation axis of the spheroid. The intensity distribution of light diffracted by a spheroid in any orientation ζ can be expressed as follows,

$$\begin{aligned} &I_S(\theta, \phi; \zeta; ka, c/a) \\ &= \pi^2(c/a)^2(ka)^4\left[\frac{2J_1(lka\sin\theta)}{lka\sin\theta}\right]^2, \end{aligned} \tag{9}$$

where

$$l = (\xi^2\cos^2\phi + \sin^2\phi)^{1/2}, \tag{10}$$

$$\xi = [(c/a)^2\sin^2\zeta + \cos^2\zeta]^{1/2}. \tag{11}$$

Here J_1 is the first order Bessel function of the first kind, and a and c are, respectively, the radius and the half-length of the rotation axis of the spheroid. For prolate spheroids ($c>a$), the azimuth angle ϕ should be measured from the long axis of the shadow ellipse, while, for oblate spheroids ($c<a$), ϕ should be measured from its short axis.

C. Superposition of the diffracted intensities over orientation

The total intensity of diffraction at an observation point for particles in different orientation is a sum of the diffracted intensity at the same point for each particle in each orientation. We consider two cases of particle orientation, namely, a case of particles oriented randomly in a 3D space on one hand, and a case in which particles are oriented randomly in a horizontal plane on the other hand (hereafter referred to as 3D random orientation and horizontal orientation, respectively). The latter is a modelling of large ice crystals falling through the atmosphere in a preferred orientation keeping their maximum dimensions horizontal (Sassen, 1980a). For both cases, each orientation in a 3D space or in a horizontal plane is supposed to occur with a uniform probability.

The diffraction intensities I_{H3} and I_{S3} for hexagonal cylinders and spheroids, respectively, in 3D random orientation are given by

$$\begin{aligned} &I_{H3}(\theta; ka, c/a) \\ &= \frac{6}{\pi^2}\int_0^{\pi}\int_0^{\pi/6}\int_0^{\pi/2} I_H(\theta, \phi; \alpha, \beta; ka, c/a) \\ &\times \cos\alpha\, d\alpha d\beta d\phi\,, \end{aligned} \tag{12}$$

and

$$\begin{aligned} &I_{S3}(\theta; ka, c/a) \\ &= \frac{2}{\pi}\int_0^{\pi/2}\int_0^{\pi/2} I_S(\theta, \phi; \zeta; ka, c/a)\sin\zeta d\zeta d\phi\,. \end{aligned} \tag{13}$$

For 3D random orientation, the diffracted intensities are naturally independent of the azimuth angle ϕ.

In Fig. 2, a configuration of horizontal orientation is shown. The direction OZ'' corresponds to the zenith direction, ε is the angle between the incident direction EO and a horizontal plane

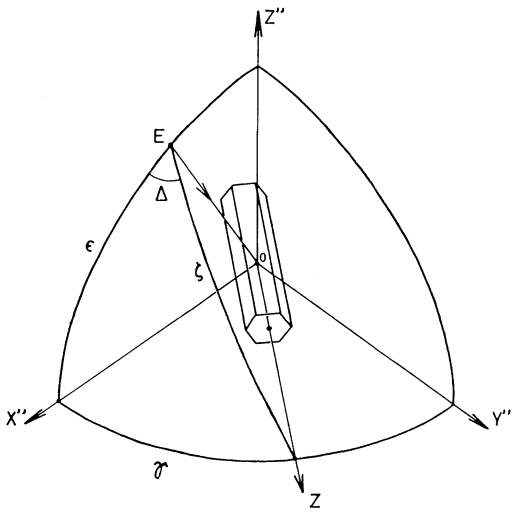

Fig. 2 Geometry for a hexagonal column oriented in a horizontal plane.

$X''OY''$, and represents the elevation angle of the incident light source. γ is the angle between the c axis of a hexagonal column or a prolate spheroid and the X'' axis; this angle describes the orientation of a particle in the horizontal direction. From the spherical trigonometry, the angles $\zeta(=\pi/2-\alpha)$ and Δ are given, respectively, by

$$\cos\zeta=\sin\alpha=\cos\varepsilon\cos\gamma, \quad (0\leqq\zeta,\ \alpha\leqq\pi/2), \tag{14}$$

$$\cos\Delta=\frac{\sin\varepsilon\cos\gamma}{\sin\zeta}. \tag{15}$$

In this case, the azimuth angle at an observation point is measured from the $X''OZ''$ plane (the principal meridional plane); we denote this azimuth angle by Φ, in order to discriminate it from ϕ measured from a body-fixed coordinate for I_H and I_S.

Considering that the angle γ takes values between 0 and 2π with an equal probability, and that at each γ a hexagonal column may rotate about its c-axis, the diffracted intensity I_{HC} for hexagonal columns in horizontal orientation can be expressed in the form:

$$I_{HC}(\theta,\Phi;\varepsilon;ka,c/a)=\frac{3}{\pi^2}\int_0^{\pi/3}\int_0^{\pi}I_H(\theta,-\phi\pm\Delta\pm\Phi;\alpha,\beta;ka,c/a)d\gamma d\beta. \tag{16}$$

For prolate spheroids in horizontal orientation, the corresponding expression for the diffracted intensity I_{PS} is written as

$$I_{PS}(\theta,\Phi;\varepsilon;ka,c/a)=\frac{1}{\pi}\int_0^{\pi}I_S(\theta,\pm\Delta\pm\Phi;\zeta;ka,c/a)d\gamma. \tag{17}$$

For planar particles such as hexagonal plates and oblate spheroids in horizontal orientation, their c axes happen to be parallel to the Z'' axis in Fig. 2: the integration over the orientation angle γ is not necessary. The diffracted intensities I_{HP} and I_{OS} for hexagonal plates and oblate spheroids in horizontal orientation are, respectively, given by

$$I_{HP}(\theta,\Phi;\varepsilon;ka,c/a)=\frac{3}{\pi}\int_0^{\pi/3}I_H(\theta,-\phi\pm\Phi;\varepsilon,\beta;ka,c/a)d\beta, \tag{18}$$

and

$$I_{OS}(\theta,\Phi;\varepsilon;ka,c/a)=I_S(\theta,\pm\Phi;\pi/2-\varepsilon;ka,c/a). \tag{19}$$

Rather complicated expressions for the azimuth angle seen in these equations (16) through (19) stem from the fact that the azimuth angles for I_H and I_S are measured from the direction fixed to the scattering body. The double sign appearing in these equations can be taken arbitrarily, and the diffracted intensities coincide with each other for any choice of the double sign. This results from the symmetrical properties of the diffraction pattern of each particle with respect to the $\phi=0°-180°$ plane, and from the randomness of orientation in a horizontal plane. In addition, one should notice in those equations that the diffracted intensities of particles in horizontal orientation depend not only on the scattering angle θ but also on the azimuth angle Φ. The azimuthal dependence has often been ignored in the foregoing studies (e.g., Liou, 1972; Stephens, 1980b; Coleman and Liou, 1981). Furthermore, the validity of the scheme proposed by Liou (1972) for integration over random orinentation is somewhat questionable; a more detailed discussion will be given in the Appendix.

D. Diffracted intensity for the forward direction

For the forward direction ($\theta=0$), the diffracted intensity of a particle is given, excluding a constant factor, by $k^4G^2(\zeta,\beta)$ from Eq. (1); $G(\zeta,\beta)$ is the geometric shadow area of the particle at the incident direction (ζ,β). For convex nonspherical particles oriented randomly in a 3D space, the diffracted intensity $I(\theta=0)$ in the forward direction is given by averaging $k^4G^2(\zeta,\beta)$ over all particle orientation. Then, from the Schwarz inequality, the following relation holds:

$$\bar{I}(\theta=0)=\frac{1}{4\pi}\int_0^{2\pi}\int_0^{\pi}k^4G^2(\zeta,\beta)\sin\zeta d\zeta d\beta \geqq\left[\frac{1}{4\pi}\int_0^{2\pi}\int_0^{\pi}k^2G(\zeta,\beta)\sin\zeta d\zeta d\beta\right]^2. \tag{20}$$

The right side of Eq. (20) is just the diffracted intensity I_0 for a spherical particle of the same surface area, or equivalently, of the cross sectional area equal to the averaged projected area of randomly oriented convex particles (van de Hulst, 1957). Equation (20) implies that the diffracted intensity for the forward direction is larger for randomly oriented convex particles than for the surface-area equivalent sphere.

As an example, we shall examine the forward diffraction intensity of hexagonal cylinders in 3D random orientation. For a hexagonal cylinder, the geometrical shadow area G_H at the incident

direction (α, β) can be expressed in the form*

$$\bar{G}_H(a, \mu; \alpha, \beta)=\frac{3\sqrt{3}}{2}a^2\sin\alpha + 4a^2\mu\cos\alpha\cos\left(\frac{\pi}{6}-\beta\right). \quad (21)$$

where

$$\mu=c/a. \quad (22)$$

Integrating over orientation, the averaged geometrical shadow area becomes

$$\bar{G}_H(a, \mu)=\frac{6}{\pi}\int_0^{\pi/6}\int_0^{\pi/2}G_H(a, \mu; \alpha, \beta)\cos\alpha d\alpha d\beta = 3a^2(\sqrt{3}/4+\mu). \quad (23)$$

Writing r_G for the radius of the surface-area equivalent sphere, the following relation between a and r_G results in,

$$\frac{a}{r_G}=\sqrt{\frac{\pi}{3(\sqrt{3}/4+\mu)}}. \quad (24)$$

From Eqs. (20), (21), and (24), we obtain

$$\bar{I}/I_0(\theta=0) = \frac{\frac{9}{4}+\frac{12\sqrt{3}}{\pi}\mu+\frac{64}{\pi}\left(\frac{\sqrt{3}}{8}+\frac{\pi}{12}\right)\mu^2}{9\left(\frac{\sqrt{3}}{4}+\mu\right)^2}>1, \quad (25)$$

where $I_0=k^4(\pi r_G^2)^2$ is adopted.

Similar expressions can be obtained for randomly oriented spheroidal particles by integrating the squares of their geometrical shadow areas (e.g., Eqs. (5) and (6) of Asano (1979)). Figure 3 shows the forward diffraction intensity ratios $\bar{I}/I_0(\theta=0)$, as a function of the shape parameter (c/a for columnar particles, i.e., hexagonal columns and prolate spheroids, and a/c for planar particles), for hexagonal cylinders and spheroids in 3D random orientation. As expected from Eqs. (20) and (25), the forward diffraction intensity of randomly oriented nonspherical particles is larger than that of the area-equivalent sphere: especially, in the limit of $c/a\to 0$, the forward diffraction by very thin planar particles tends to be 1.33 times more intense than for the equivalent sphere.

E. Similarity of the diffracted intensities

An another interesting feature is a similarity in the diffracted intensities of particles of different sizes but with a same shape. The geometric shadow area and the diffracted intensity of a hexagonal cylinder with a size ρ times larger but of the same shape are expressed in terms of those for the original cylinder as,

$$G_H(\rho a, \mu; \alpha, \beta)=\rho^2 G_H(a, \mu; \alpha, \beta), \quad (26)$$

$$I_H(\theta, \phi; \alpha, \beta; \rho ka, c/a) = \rho^4 I_H(\theta^*, \phi; \alpha, \beta; ka, c/a), \quad (27)$$

with

$$\theta^*=\sin^{-1}(\rho\sin\theta). \quad (28)$$

The same similarity holds for spheroidal particles. This similarity relation provides a useful method to estimate the diffraction intensity of particles of different sizes but with a same shape.

Now we shall introduce the normalized intensity I^N defined as

$$I^N=I/(\pi k^2 G). \quad (29)$$

Then, from Eqs. (26) and (27), we have

$$I^N(\theta, \phi; \alpha, \beta; \rho ka, c/a) = \rho^2 I^N(\theta^*, \phi; \alpha, \beta; ka, c/a). \quad (30)$$

The normalized intensity I^N satisfies the following normailzation condition,

$$\frac{1}{\pi}\int_0^{\pi}\int_0^{\pi/2} I^N \sin\theta d\theta d\phi = 1. \quad (31)$$

The similarity relation Eq. (30) is also valid even for the diffracted intensities integrated over a size distribution such as the modified gamma

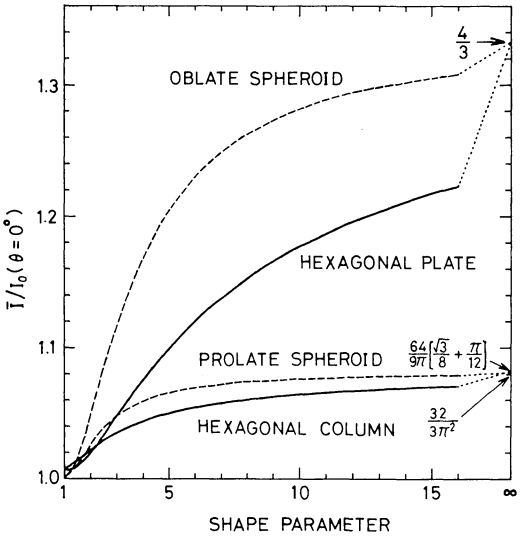

Fig. 3 Ratios of the diffracted intensities of randomly oriented hexagonal cylinders and spheroids to that for the surface-area equivalent sphere at $\theta=0°$.

* In the right side of Eq. (9) of Coleman and Liou (1981), the factor L/3 should be read as 2L/3, then the expression becomes equivalent to ours.

distribution or the log-normal distribution, when the mean size is varied but the variance of distributions remains unchanged. This can be easily shown by invoking that the above size distributions have the following property:

$$n(x, \rho x_e, v)=\frac{1}{\rho} n\left(\frac{1}{\rho} x, x_e, v\right), \qquad (32)$$

where the notation is explained in the next section.

3. Computed results

In order to check correctness of our formulation, the diffraction pattern, computed by Eq. (8), of a regular hexagonal aperture was compared with some photographic images of the Fraunhofer diffraction by the similar apertures (Smith and Marsh, 1974; Scheiner and Hirayama, 1894). The computed diffraction pattern agrees well with the images. Figure 4 shows the intensity distribution diffracted by a hexagonal cylinder of $c/a=2$ and $k^2G=10^4$, for the orientation of $\alpha=60°$ and $\beta=20°$. The shape of the projected shadow of the cylinder is depicted at the upper right corner. At scattering angles $\theta \gtrsim 3°$, the maximum intensity appears at $\phi \simeq 165°$ and 345° (roughly parallel to the short sides of the geometric shadow), and the secondary maximum appears at $\phi \simeq 75°$ and 255° (parallel to the long sides of the geometric shadow), while in the intermediate azimuthal directions the diffracted intensity becomes minimum. For round particles like spheroids, the azimuthal distribution pattern is much more smooth; the diffraction pattern of a spheroid is elliptical.

Next, we computed the diffracted intensity of hexagonal cylinders in 3D random orientation. For a comparison with the result by Coleman and Liou (1981, Fig. 6), the normalized intensities diffracted by the same particles are shown in Fig. 5, as a function of the scattering angle θ. The size parameter for the wavelength $\lambda=0.55\mu$m is about 19 times larger than for $\lambda=10.6\mu$m. Following the similarity relation discussed above, the normalized intensity in the forward direction at $\lambda=0.55\mu$m should be about 360 times larger than that at $\lambda=10.6\mu$m, just as shown in the figure. In contrast, Coleman and Liou obtained the forward scattering intensities of the same order of magnitude at the both wavelengths.

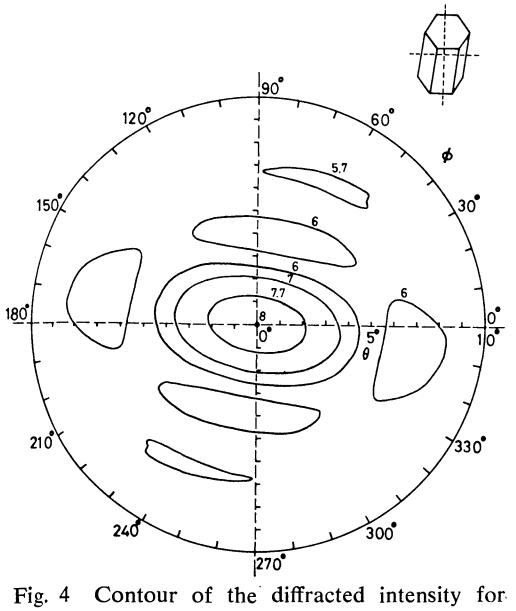

Fig. 4 Contour of the diffracted intensity for a hexagonal cylinder of $c/a=2$ and $k^2G=10^4$ at the specific orientation $(\alpha, \beta)=(60°, 20°)$. The insert at the upper right corner is the geometric shadow of this hexagonal cylinder. Numerical values denote the logarithms of the intensities of the diffracted light.

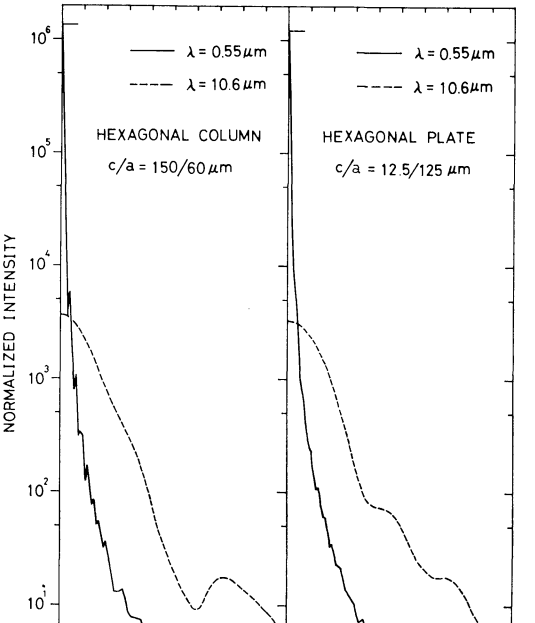

Fig. 5 Normalized diffracted intensities for hexagonal cylinders in 3D random orientation at two wavelengths $\lambda=0.55\mu$m and 10.6μm.

As seen on the curves for $\lambda=10.6\mu$m in Fig. 5, some conspicuous fluctuations still remain even after averaging over random orientation. Integration over a particle size distribution was performed in order to smooth out the fluctuations. The modified gamma distribution function was used in the form:

$$n(x, x_e, v)=\frac{(x_e v)^{(2v-1)/v}}{\Gamma\left(\frac{1-2v}{v}\right)}x^{(1-3v)/v}\times\exp\left(-\frac{x}{x_e v}\right), \quad (33)$$

where $n(x, x_e, v)dx$ is the number of particles with the size parameters between x and $x+dx$, x_e is the effective size, v is the effective variance, and Γ is the gamma function. In the integration, the particle shape c/a was kept constant.

In Fig. 6, the normalized intensities of diffraction by hexagonal columns and plates in 3D random orientation are compared with those for the surface area equivalent spheres. The corresponding figure for prolate and oblate spheroids is given in Fig. 7. In both figures, the geometric shadow area $k^2\widetilde{G}$ averaged over orientations and sizes is set to be $\pi(100)^2$. The diffraction intensity patterns of planar particles are much more closer to those of the spheres than those of columnar particles are. This is because, for planar particles, the geometric shadow area is larger when the shape of geometric shadow is closer to spherical, and vice versa for columnar particles. For forward scattering, however, the columnar particles have the diffracted intensities closer to that of the equivalent spheres than the planar particles do, as already shown in Fig. 3. It is worth noting that the diffracted intensities of hexagonal cylinders and spheroids of the same aspect ratio resemble each other. This similarity results from averaging the diffracted intensities over all orientation. This result suggests that spheroids are a useful substitute to approximate the diffraction by hexagonal cylinders in 3D random orientation: computational task for spheroids is much less than for hexagonal cylinders.

Figures 8 to 11 display the distribution patterns of the diffracted intensity for hexagonal cylinders and spheroids oriented randomly in a horizontal plane. Since the diffracted intensity is symmetrical with respect to the $\Phi=0°-180°$ plane, and the $\Phi=90°-270°$ plane,* the dif-

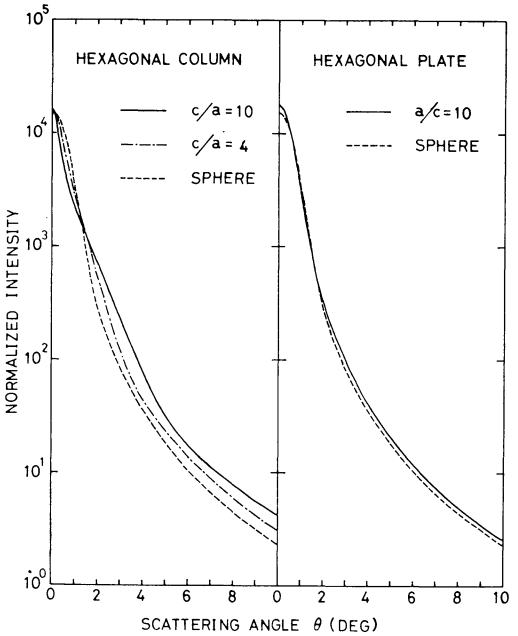

Fig. 6 Normalized diffracted intensities for polydispersed hexagonal cylinders in 3D random orientation. $k^2\widetilde{G}=\pi(100)^2$, $v=0.1$.

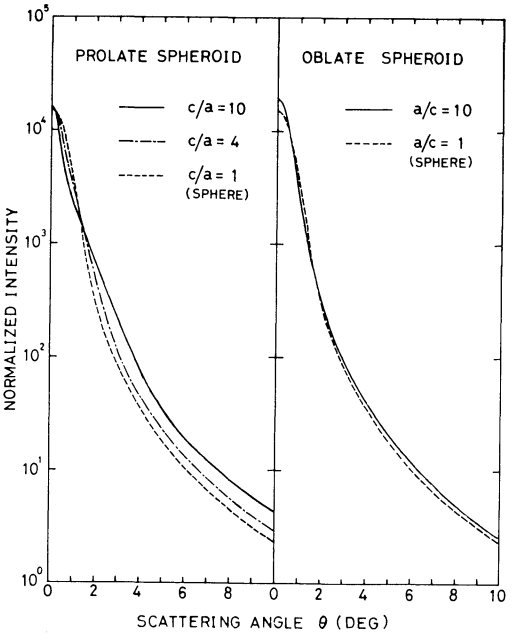

Fig. 7 Normalized diffracted intensities for polydispersed spheroids in 3D random orientation. $k^2\widetilde{G}=\pi(100)^2$, $v=0.1$.

* We can obtain the former symmetry by replacing Φ with $-\Phi$ in Eqs. (16) through (19), and the latter symmetry by replacing Φ with $\pi-\Phi$ in the symmetry relation $I_H(\theta, \phi; \alpha, \beta; ka, c/a)=I_H(\theta, \phi\pm\pi; \alpha, \beta; ka, c/a)$.

fraction pattern only in one quardrant is shown. In these figures, the diffracted intensities are normalized by $\pi(300)^2$. Contours of this quantity are drawn at every half order of magnitude.

Figure 8 shows contours of the diffracted intensities at the source (e.g., the sun) elevation angle of $\varepsilon=10°$. For oblate spheroids, the distribution pattern is elliptical: the aspect ratio of the elliptical pattern is given, from Eqs. (11) and (19), by

$$\xi^*=\left[\sin^2\varepsilon+\left(\frac{c}{a}\right)^2\cos^2\varepsilon\right]^{-1/2}. \tag{34}$$

For prolate spheroids, the contours slightly deviate from elliptical patterns.

At very low sun elevations, the geometric shadows of hexagonal plates take nearly rectangular forms whose long sides are horizontal. As inferred from Fig. 4, the diffracted intensity of a rectangular aperture will have minima in its diagonal directions. Thus, for hexagonal plates in horizontal orientation, the diffraction pattern at the low sun elevation ($\varepsilon=10°$) becomes concave in intermediate Φ directions, and tends to look like a cross. On the other hand, for hexagonal columns, the diffraction pattern resembles an asteroid or a rhombus. This is because many different diffraction patterns are superposed for the case of hexagonal columns.

Figure 9 shows the diffraction patterns of the same particles as in Fig. 8, but for the sun elevation $\varepsilon=30°$. For higher sun elevation angles, the diffraction pattern, as a whole, becomes less conspicuous though the characteristic features mentioned in Fig. 8 are still conserved. Note that at the limiting case of $\varepsilon=90°$, the diffraction pattern for particles in horizontal orientation is isotropic with respect to Φ with isolines forming concentric circles.

In the lower halves of Figs. 8, 9, and 10, demonstrated is an effect of the variance v of size distributions on the diffraction patterns of spheroidal and hexagonal particles in horizontal orientation. Calculations for different values of v indicate that if the variance v is large enough to smooth out fluctuations in the diffracted intensities, it does not significantly change the diffraction patterns.

The upper half of Fig. 10 shows the diffraction patterns, at two elevations $\varepsilon=10°$ and 30°, for a mixture of hexagonal plates and columns in horizontal orientation as well as spherical particles; these particles are mixed with an equal proportion. The spherical particles here are supposed to simulate such ice crystals having spatial structures as bullet rosettes. Such ice crystals may be oriented randomly in a 3D space regardless of their sizes. The concave contours of hexagonal plates are almost compensated by the

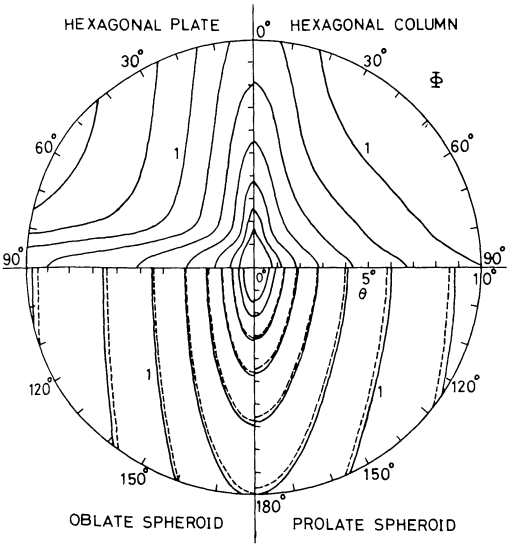

Fig. 8 Distributions of the normalized diffracted intensities for hexagonal cylinders and spheroids in horizontal orientation. $\varepsilon=10°$, $SP=4$, $k^2\tilde{G}=\pi(300)^2$. The solid and broken lines correspond to the cases of $v=0.1$ and $v=0.2$, respectively.

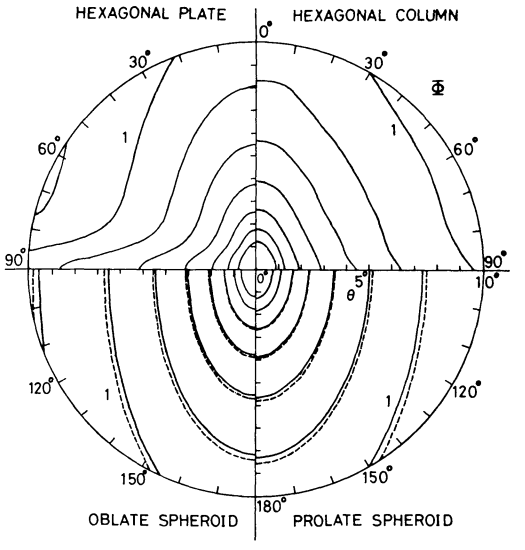

Fig. 9 Same as Fig. 8 but for $\varepsilon=30°$. The solid and broken lines correspond to the cases of $v=0.2$ and $v=0.1$, respectively.

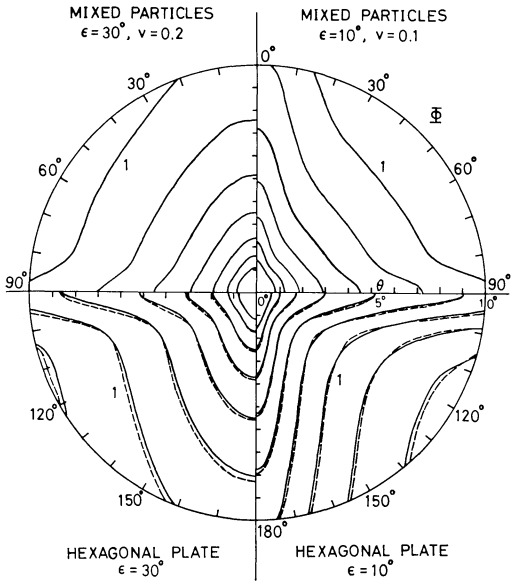

Fig. 10 Distributions of the normalized diffracted intensities for mixed particles and hexagonal plates in horizontal orientation. $SP=4$, $k^2\tilde{\tilde{G}}=\pi(300)^2$. The solid and broken lines in the lower half correspond to the cases of $v=0.2$ and $v=0.1$, respectively.

circular contours of spherical particles, then the diffraction patterns just like those for hexagonal colmuns in Figs. 8 and 9 result for the mixtures. This implies that we can hardly discriminate horizontally oriented hexagonal columns from a mixture of various ice crystals only from their diffraction patterns.

The Reynolds number R_e of planar ice crystals falling in the atmosphere was estimated by Sassen (1980a). He concluded that planar ice crystals in the range $1.0<R_e<100$ are in stable horizontal orientation. On the basis of Kajikawa (1972) and Heymsfield (1972), we estimated the averaged maximum dimensions and the Reynolds numbers of hexagonal cylinders of $k^2\tilde{\tilde{G}}=\pi(300)^2$ used in this calculation (see Table 1). Here we take the visible wavelength $\lambda=0.7\mu$m and the variance $v=0.1$. For the hexagonal plates, R_e is too small to satisfy Sassen's condition for horizontal orientation. So we extended calculations to hexagonal plates of $k^2\tilde{\tilde{G}}=\pi(600)^2$. In this case, R_e is 1.9 and about 1.3 for the shape parameters $SP=4$ and 10, respectively. Figure 11 shows the diffraction patterns of these hexagonal plates in horizontal orientation for source elevation angles $\varepsilon=10°$ and 30°. As expected from the similarity relations in the section 2-E, the diffraction patterns for the hexagonal plates of $k^2\tilde{\tilde{G}}=\pi(600)^2$ and $\pi(300)^2$ are quite similar to each other: the directly calculated values of the diffracted intensity for $k^2\tilde{\tilde{G}}=\pi(600)^2$ at small scattering angles agreed with the estimated values obtained using the similarity relations from those for $k^2\tilde{\tilde{G}}=\pi(300)^2$.

Table 1 Average maximum dimensions of hexagonal cylinders under consideration at the wavelength $\lambda=0.7\mu$m and the Reynolds numbers.

	$SP=4$	$SP=10$
column	$2\bar{c}=123\ \mu$m $R_e=1.8$	$2\bar{c}=200\ \mu$m $R_e\simeq 1.0$
plate	$2\bar{a}=78\ \mu$m $R_e=0.3$	$2\bar{a}=88\ \mu$m $R_e\simeq 0.3$

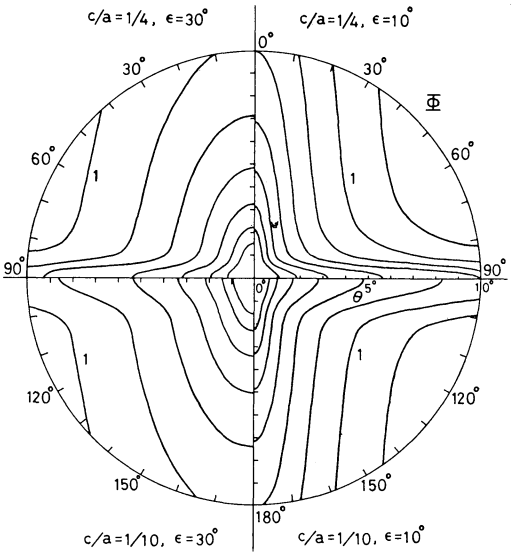

Fig. 11 Distributions of the diffracted intensities for hexagonal paltes in horizontal orientation. $k^2G=\pi(600)^2$, $v=0.1$.

4. Application to optical phenomena due to ice crystals

Sassen (1980b) displays a photograph of a moonrise accompanied by the moon pillar and "moon dogs". Since the parhelia (moon dogs), without the 22° halo and upper tangent arc, can be seen in the picture, the suspended ice crystals at that time might be hexagonal plates oriented randomly, keeping their basal planes nearly horizontal. The author attributed the light pattern

in the vicinity of the moon to a light cross caused by a combination of a light pillar above and beneath the moon with a segment of the horizontal parhelic circle. According to Lynch (1979), however, the intensity of the parhelic circle is of the minimum in the direction of the light source at any source elevation. Therefore the light stripe in the horizontal direction looks like a diffraction pattern rather than a segment of the parhelic circle. Figures 8 and 11 suggest that the vertical light stripe may also result partly from the diffraction, at least in the extreme vicinity of the moon. In general, the light cross has so far been explained as a combination of the light pillar and the parhelic circle (e.g., Minnaert, 1954). Here we suggest that the light cross, at least at low source elevations, can partly be due to a diffraction pattern of hexagonal plate crystals in horizontal orientation.

Non-isotropic diffraction patterns with respect to the azimuthal direction have been observed by many investigators. For example, in the picture of a surface halo (Plate 19 of Kuhn (1978)), the diffraction pattern concave for intermediate Φ directions can be seen. Since the 22° halo ring caused by freshly fallen ice crystals appears on the ground, the sun elevation might be less than 22°. From the anisotropic diffraction pattern, without any other optical phenomena in the atmosphere, we can infer that large plate crystals might have been suspended in horizontal orientation at that time. Simultaneous occurrance of optical phenomena such as the 22° halo, parhelia, and upper tangent arc is frequently observed, and their photographs have been displayed by, for example, Evans and Tricker (1972, Fig. 3), Greenler (1980, Plate 2-18), and Tricker (1972). Then sun elevation angles were about 14, 20, and 30°, respectively, in those pictures. From these pictures, we can suppose a simultaneous presence of hexagonal planar and columnar crystals in horizontal orientation and of ice crystals in 3D random orientation. The diffraction patterns in these pictures look like a rhombus or an asteroid for the former two cases, and a dumpy rhombus for the last case: the patterns agree well with the calculated diffraction patterns for mixed particles in Fig. 10. The diffraction pattern recognition may also be useful to infer types and fall attitudes of ice crystals in such cases where ice crystals have no definite hexagonal structures or clear optical faces causing appreciable optical phenomena, and where ice clouds are too thin to produce optical phenomena.

In calculations for horizontal orientation, we assumed a complete random orientation in a horizontal plane. In the atmosphere, however, falling ice crystals may flutter, more or less, about their stable horizontal orientation. This wobbling may cause a horizontal and/or vertical extension of optical phenomena, as well as a blurring of the diffraction patterns predicted by calculations.

5. Conclusions

The explicit formulas for the Fraunhofer diffraction by a hexagonal cylinder and a spheroidal particle in any arbitrary orientation have been derived. The computed diffraction patterns agreed quite well with photographic images of the Fraunhofer diffraction pattern (Smith and Marsh, 1974; Scheiner and Hirayama, 1894).

Calculations for completely random orientation in a 3D space indicate that diffraction by randomly oriented hexagonal cylinders can be approximated by that of spheroids of the same shape parameter. For horizontally random orientation, the diffracted intensity is a function not only of the scattering angle but of the azimuth angle. The diffraction patterns of hexagonal cylinders in horizontal orientation strongly depend on the elevation angle of light source; the diffraction patterns are highly anisotropic with respect to the azimuthal direction at low source elevations.

Applications to optical phenomena due to ice crystals in the atmosphere were discussed. A suggestion is made that the light cross at low source elevations may be due to diffraction by hexagonal planar crystals in horizontal orientation rather than due to a combination of a light pillar and a parhelic circle. A utility of diffraction to infer shapes and fall attitudes of ice crystals in the atmosphere has been pointed out. For further studies, it is desirable to combine an analysis of the diffraction patterns with a simultaneous sampling of such ice crystals as diamond dusts causing the diffraction near the ground at the polar regions.

Acknowledgements

We wish to thank Prof. M. Tanaka for his encouragement throughout this work. We are grateful to Dr. K. Kawabata for his critical reading of the manuscript.

Note added in proof

After submission of this work, we came across the papers by Komrska, J., 1972: *Opt. Acta,* **19**, 807-816 and 1973: *Opt. Acta,* **20**, 549-563, where, prior to the work of Smith and Marsh, the computed Fraunhofer diffraction patterns for some regular polygonal apertures have been compared with the experimental profiles.

Appendix

Liou (1972) defined an averaged quantity $\bar{F}(\theta)$ over random orientation in a 3D space as

$$\bar{F}=\frac{2}{\pi^2}\int_0^{\pi}\int_0^{\pi/2}F(\varepsilon,\gamma)d\varepsilon d\gamma\,, \tag{A1}$$

where $F(\varepsilon, \gamma)$ is a physical quantity depending on the elevation angle ε and the orientation angle γ (see Fig. 2). This scheme has been adopted by several investigators to calculate averaged values over random orientation (Stephens, 1980a; Coleman and Liou, 1981). Taking the projected shadow area of a prolate spheroid as the physical quantity, we evaluated the averaged shadow area over 3D random orientation both by Eq. (A1) and by our scheme Eq. (13). The projected shadow area of a prolate spheroid of size ka and $\mu=c/a$ in an orientation (ε, γ) is written in the form (Asano, 1979):

$$\begin{aligned}G(a,\mu;\varepsilon,\gamma)&=\pi(ka)^2[\mu^2\sin^2\zeta+\cos^2\zeta]^{1/2}\\&=\pi(ka)^2[\mu^2-(\mu^2-1)\cos^2\varepsilon\cos^2\gamma]^{1/2}.\end{aligned} \tag{A2}$$

Our scheme Eq. (13) gives

$$\bar{G}=\frac{\pi}{2}a^2\left[1+\frac{\mu^2}{\sqrt{\mu^2-1}}\sin^{-1}\left(\frac{\mu^2-1}{\mu}\right)\right], \tag{A3}$$

which is exactly equal to 1/4 of the surface area of the spheroid: the average geometrical shadow area of identical convex particles in 3D random orientation is one-fourth their surface area (van de Hulst, 1957). For $\mu=4$, for example, Equation (A3) gives $\bar{G}=3.223\pi a^2$. On the other hand, numerical evaluation of Eq. (A1) for the same prolate spheroid yields $\bar{G}=3.426\pi a^2$, which is a little larger than the exact value. Thus, the scheme (A1) does not accurately represent the average over 3D random orientation.

References

Asano, S., 1979: Light scattering properties of spheroidal particles. *Appl. Opt.,* **18**, 712-723.

Born, M. and E. Wolf, 1975: *Principles of Optics.* Pergamon Press. 385, 396 pp.

Cai, Q. and K. N. Liou, 1982: Polarized light scattering by hexagonal ice crystals: Theory. *Appl. Opt.,* **21**, 3569-3580.

Coleman, R. F. and K. N. Liou, 1981: Light scattering by hexagonal ice crystals. *J. Atmos. Sci.,* **38**, 1260-1271.

Evans, W. F. J. and R. A. R. Tricker, 1972: Unusual ares in the Saskatoon halo display. *Weather,* **27**, 234-238.

Greenler, R. G., 1980: *Rainbows, halos, and glories.* Cambridge Univ. Press.

Heymsfield, A., 1972: Ice crystal terminal velocities. *J. Atmos. Sci.,* **29**, 1348-1357.

Jacobowitz, H., 1971: A method for computing the transfer of solar radiation through clouds of hexagonal ice crystals. *J. Quant. Spectrosc. Radiat. Transfer,* **11**, 691-695.

Kajikawa, M., 1972: Measurement of falling velocity of individual snow crystals. *J. Meteor. Soc. Japan,* **50**, 577-584.

Kuhn, M., 1978: Optical phenomena in the Antarctic Atmosphere. *Meteorological Studies at Plateau Station, Antarctica, Antarctic Research Series,* **25**, 129-155.

Liou, K. N., 1972: Light scattering by ice clouds in the visible and infrared: A theoretical study. *J. Atmos. Sci.,* **29**, 524-536.

Lynch, D. K., 1979: Polarization models of halo phenomena. 1. The parhelic circle. *J. Opt. Soc. Am.,* **69**, 1100-1103.

Minnaert, M., 1954: *The nature of light and color in the open air.* Dover Pub. p. 202.

Sassen, K., 1980a: Remote sensing of planar ice crystal fall attitudes. *J. Meteor. Soc. Japan,* **58**, 422-429.

————, 1980b: Light pillar climatology: A study in microphysics at Laramie, Wyoming. *Weatherwise,* **33**, 259-262.

Scheiner, J. and S. Hirayama, 1894: Photographische Aufnahmen Fraunhofer'scher Beugungsfiguren. *Abh. Konigl. Akad. Wiss., Berlin,,* Anhang 1, 1-13.

Smith, R.C. and J. S. Marsh, 1974: Diffraction patterns of simple apertures. *J. Opt. Soc. Am.,* **64**, 798-803.

Stephens, G. L., 1980a: Radiative properties of cirrus clouds in the infrared region. *J. Atmos. Sci.,* **37**, 435-446.

————, 1980b: Radiative transfer on a linear lattice: Application to anisotropic ice crystal clouds. *J. Atmos. Sci.,* **37**, 2095-2104.

Tricker, R. A. R., 1972: Observations on certain features to be seen in a photograph of haloes taken by Dr. Emil Schulthess in Antarctica. *Quart. J. R. Meteor. Soc.,* **98**, 542-562.

van de Hulst, H. C., 1957: *Lgiht Scattering by Small*

Particles. Wiley, 105, 110 pp.
Wendling, P., R. Wendling and H.K. Weickmann, 1979: Scattering of solar radiation by hexagonal ice crystals. *Appl. Opt.*, **18**, 2663-2671.

大気中に浮遊する氷晶による光の Fraunhofer 回折

高　野　精　秀
東北大学理学部超高層物理学研究施設

浅　野　正　二
気象研究所高層物理研究部

任意の方向を向いた有限の長さの六角柱および回転楕円体の Fraunhofer 回折の定式化を行い，3次元空間内および水平面内にランダムに方位する各々の粒子の回折強度を計算した。3次元空間内にランダムに方位する六角柱の回折強度は，同じ縦横比の回転楕円体のそれによってうまく近似される。粒子が水平面内に長軸を保って方位する場合の回折強度は散乱角だけではなく方位角の関数でもあり，六角柱と回転楕円体で回折パターンはかなり違う。水平面方位した六角柱の回折強度分布は光源の高度に強く依存し，光源の高度が低いとき方位角について著しく異方性を示す。さらに得られた計算結果の氷晶によって生ずる大気光学現象への応用についても議論した。